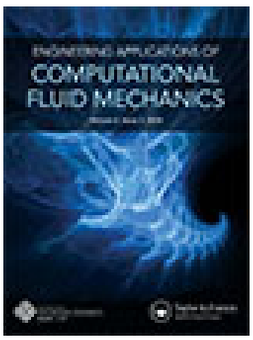

Engineering Applications of Computational Fluid Mechanics

ISSN: 1994-2060 (Print) 1997-003X (Online) Journal homepage: http://www.tandfonline.com/loi/tcfm20

Applications of Lattice Boltzmann Method to Turbulent Flow Around Two-Dimensional Airfoil

Xiao-Peng Chen

To cite this article: Xiao-Peng Chen (2012) Applications of Lattice Boltzmann Method to Turbulent Flow Around Two-Dimensional Airfoil, Engineering Applications of Computational Fluid Mechanics, 6:4, 572-580, DOI: 10.1080/19942060.2012.11015443

To link to this article: http://dx.doi.org/10.1080/19942060.2012.11015443

Published online: 19 Nov 2014.

Engineering Applications of Computational Fluid Mechanics Vol. 6, No. 4, pp. 572–580 (2012)

APPLICATIONS OF LATTICE BOLTZMANN METHOD TO TURBULENT FLOW AROUND TWO-DIMENSIONAL AIRFOIL

Xiao-Peng Chen

School of Mechanics, Civil Engineering and Architecture, Northwestern Polytechnical University, Xi'an, Shaanxi, P.R.China, 710072
E-Mail: xchen76@nwpu.edu.cn (Corresponding Author)

ABSTRACT: Lattice Boltmzann method (LBM) has been developed as an important technique of computational fluid mechanics. Two-dimensional turbulent flow around NACA0012 airfoil, with Re=10^5 and AOA=4° (angle of attack), is simulated with "multiple-relaxation time" lattice Boltzmann method incorporated with Spalart-Allmaras (SA) turbulence model. From the viewpoint of industrial applications, the related computational aspects are discussed, such as treatments of wall boundary, far field boundary conditions, and the position of the airfoil in the domain. Meanwhile, to balance the computational loads and accuracy of the simulations, grid refinement is applied. According to the results, LBM gives pretty good predictions, and quite flexible domain size can be accepted if the far field boundary condition is well posed. Compared to 3D LES-LBM simulations, two-dimensional LBM with SA turbulent model is of lower computational load, but with good accuracy.

Keywords: lattice Boltzmann methods, Spalart-Allmaras model, grid refinement, interpolated bounce-back boundary scheme, turbulence

1. INTRODUCTION

Lattice Boltzmann method (LBM) has received considerable interest in the past decades as an efficient method of computing a variety of fluid flows, ranging from low-Reynolds-number flows to highly turbulent flows (Chen and Doolen, 1998; Filippova et al., 2001). Meanwhile, incorporated with corresponding models, it was applied to numerous interdisciplinary fields, such as multiphase flow (Chen et al., 2011), natural convection (Scagliarini et al., 2010), etc. Early lattice Boltzmann with single relaxation time (SRT) model suffered great difficulties for large Reynolds number flow due to numerical instability (Chen and Doolen, 1998). d'Humieres (2002) proposed multiple relaxation time (MRT) LB model, where the moments of the density populations relaxed independently. It improves the feasibility of LBM for large Reynolds number flow by suppressing the short-length pressure wave with adjustable bulk viscosity (d'Humieres, 2002; Lallemand and Luo, 2003a). On the other hand, by introducing turbulent viscosity, the stability of the method could be improved. LBM is supposed to be superior to conventional N-S equation based CFD method on turbulent flow (Chen et al., 2003). First of all, LBM can present rich and complex physics when projected onto hydrodynamic variables in x space. Second, both turbulent and thermal fluctuations are coupled at the same level. Third, the parameter - relaxation time, τ- naturally includes both the regular viscous effects and its higher order modifications. In recent years, LBM based Direct Numerical Simulations (DNS), Large Eddy Simulations (LES) (Premnath et al., 2009; Liu et al, 2012), Reynolds-Averaged Navier-Stokes calculations (Filippova et al., 2001; Zhuo et al., 2010) were implemented, which showed great success in turbulence predictions. Both DNS and LES require 3D simulation and comparatively fine grid resolution. That implies heavy computational loads. It will be expensive for preliminary industrial design or for interdisciplinary research, such as turbulent multiphase flows. The goal of this paper is to demonstrate the feasibility of RANS coupled LBM simulation. And relative numerical models and techniques will be discussed as well.

During the past decades, different LBM simulation techniques were developed widely, which laid solid foundations for further applications. To date, commercial software (like PowerFLOW) and open source codes (like Palabos) have appeared. For industrial applications, the boundary conditions and grid configurations are always the key issues of successful simulations. Some of them borrowed ideas from conventional methods. For instance, density filtering and characteristic boundary conditions for LBM were proposed as non-

Received: 28 Nov. 2011; Revised: 9 Jun. 2012; Accepted: 28 Jun. 2012

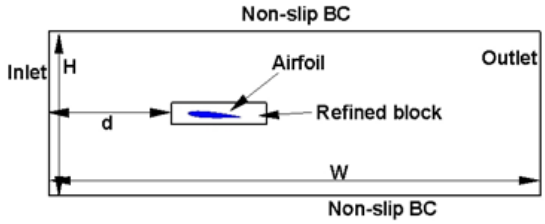

Fig. 1 Schematic diagram of computational model.

reflective far field conditions. The performances of them were analyzed in depth by Kam et al. (2007) and Estallo (2008). On the other hand, rooting in the essence of mesoscopic particle kinetics, wall boundary (Chen and Doolen, 1998) and grid refinement treatments (Chen et al., 2006; Zhuo et al., 2010) were designed specifically. For the former one, bouncing-back (including interpolated bounce-back), non-equilibrium extrapolation etc. were proposed. Recent asymptotic analysis (Shankar and Sundar, 2009) showed most of them (or their modified version) were of second order accuracy, the same as LBM. While for grid refinement method, interpolation (Yu et al., 2003) and controlled element schemes (Chen et al., 2006) were developed.

In this paper, MRT-LBM coupled with SA turbulent model is applied to two-dimensional flow around NACA0012 airfoil. In the framework of block-based Cartesian grid, the boundary conditions, parameters of calculations and strategies are discussed in details. In section 2, the computation models and various aspects of computation are introduced. In section 3, the results are presented and discussed. Conclusions are drawn in section 4.

2. NUMERICAL MODEL AND METHODS

2.1 Physical model

The computational model is sketched in Fig 1. In the model, NACA0012 airfoil is under an angle of attack (AOA) of 4°. Reynolds number of the flow is set as 10^5 as in Counsil and Boulama (2011), where inlet velocity (u_{inlet}) and cord length (c) are used as characteristic values. In the most of tested cases, the height (H) and width (W) of the computational domain are 1600 and 1800 lattice size, respectively. And the refined block covers the area of 450~800 × 760~840 in x and y direction, respectively. The ratio of fine grid size to coarse one is 0.25. Fixed velocity (u_{inlet}) and pressure (p_{out}) are imposed on inlet and outlet boundaries, respectively, with special treatment to reduce reflective waves, which will be described in section 2.5. Slipping boundary condition is imposed on the upper and lower boundaries.

2.2 MRT - LBM and Spalart-Allmaras turbulent model

Lattice Botlzmann method roots in mesoscopic particle kinetics. The governing generalized lattice Boltzmann equation reads

$$f_i(\boldsymbol{x}+\boldsymbol{c}_i\delta t, t_n+\delta t) - f_i(\boldsymbol{x}, t_n) = C\cdot\left(f_i^{eq}(\boldsymbol{x}, t_n) - f_i(\boldsymbol{x}, t_n)\right) \quad (1)$$

where C denotes the collision matrix, and f the distribution function. Maxwell equilibrium functions, f_i^{eq}, is adopted. The subscripts i depends on the lattice model (i = 0, 1…8 for D2Q9). The equation can be further transformed from the populationspace to moment space, $|m\rangle = M\cdot|f\rangle$(d'Humieres 2002, Lallemand and Luo 2003a). One of the moment spaces could be chosen as, $|m\rangle = \left(\rho, e, \epsilon, j_x, q_x, j_y, q_y, p_{xx}, p_{xy}\right)^T$. Among these nine moments, the density ρ and themomentum $\boldsymbol{j} = (j_x, j_y)$are conserved moments for the athermal LBE model. The other six moments, e, ϵ, q=(q_x, q_y), p_{xx} and p_{xy} are related to the energy, energy square, heatflux, and the diagonal and off-diagonal components of the stress tensor, respectively. Inthe equation, the collision term is transformed as, $\hat{S} = M\cdot C\cdot M^{-1} = diag\,(s_0, s_1, s_2, s_3, s_4, s_5, s_6, s_7, s_8)$. For D2Q9 model, shear and bulk viscosity are as follows.

$$\nu = \frac{1}{3}\left(\frac{1}{s_7}-\frac{1}{2}\right)c\delta x, \qquad \varsigma = \frac{1}{6}\left(\frac{1}{s_1}-\frac{1}{2}\right)c\delta x. \quad (2)$$

Applying Boussinesq hypothesis, the Reynolds stress is supposed to relate the mean velocity gradients through turbulent viscosity, ν_t. Spalart (2000) introduced an intermediate variable $\tilde{\nu} = \nu_t/f_{v1}$ with the controlled equation of

$$\frac{D\tilde{\nu}}{Dt} = C_{b1}(1-f_{t2})\tilde{S}\tilde{\nu} + \frac{1}{\sigma}\left[\nabla\left((\nu_0+\tilde{\nu})\nabla\tilde{\nu}\right) + C_{b2}(\nabla\tilde{\nu})^2\right] - s\left(C_{w1}f_w - \frac{C_{b1}}{\kappa^2}f_{t2}\right)\left(\frac{\tilde{\nu}}{dw}\right)^2 \quad (3)$$

where $f_{v1} = \frac{\chi^3}{\chi^3+C_{v1}^3}$, $\chi = \frac{\tilde{\nu}}{\nu_0}$, ν_0 is molecular viscosity, and, dw is the distance between the fluid node and wall. Other parameters are listed as follows,

$$f_{t2} = C_{t3} exp(-C_{t4}\chi^2),$$
$$\tilde{S} = \sqrt{2\Omega_{ij}\Omega_{ij}} f_{v3} + \frac{\tilde{\nu}}{\kappa^2 d^2} f_{v2},$$
$$\Omega_{ij} = \frac{1}{2}\left(\frac{\partial u_i}{\partial x_j} - \frac{\partial u_j}{\partial x_i}\right),$$
$$f_{v2} = \left(1 + \frac{\chi}{C_{v2}}\right)^{-3}, f_{v3} = \frac{(1+\chi f_{v1})(1-f_{v2})}{\chi}, \quad (4)$$
$$C_{v2} = 5, \chi = \max(\chi, 10^{-4}),$$
$$f_w = g\left(\frac{1+C_{w3}^6}{g^6+C_{w3}^6}\right)^{1/6},$$
$$g = r + C_{w2}(r^6 - r), r = \frac{\tilde{\nu}}{\tilde{S}\kappa^2 dw^2}.$$

And the corresponding constants are: $C_{b1} = 0.1355$, $C_{b2} = 0.622$, $\sigma = 2/3$, $\kappa = 0.41$, $C_{v1} = 7.1 C_{t3} = 1.1$, $C_{t4} = 2$, $C_{w1} = \frac{C_{b1}}{\kappa^2} + \frac{1+C_{b2}}{\sigma}$, $C_{w2} = 0.3$ and $C_{w3} = 2$. Then the total viscosity reads,

$$\nu = \nu_t + \nu_0 \quad (5)$$

Back to the LBM and Eq. 2, the relaxation parameter can be incorporated into flow through modified total viscosity.

2.3 Grid refinement method

In the current study, volumetric formulation based grid refinement is applied. The basic advantage of it is mass conservation. On the other hand, no interpolation procedure is needed, and therefore, it will be easy for code implementation for multi-dimensional problems. It has been successfully applied in the commercial software, PowerFLOW, and the robustness has been demonstrated. While for others, like interpolation scheme, highly oscillating distributions might cause computational instability, and the grid Reynolds number ($U\delta x/\nu$) should be checked carefully.

In the scope of volumetric formulation based grid refinement approach, the particle distributions locate at the center of each computational cell. With constraint of conservation, the variables can be exploded and coalesced freely between corresponding coarse and fine grid sets. Since both grids are uniformly constructed, standard LBM procedure can be applied. It comprises the following steps,

1. Explode. The particle distributions are redistributed from coarse to fine grid cells, homogeneously or cording to their gradients on coarse grid.
2. Advect on fine and coarse grids. Standard propagation step is performed on interior grid, while on the coarse-refine grid interface, distributions are interchanged: particles originating from the coarse grid remain unchanged and simply propagate to the fine grid.
3. Collide on fine grid. After this step, the densities on $\tilde{t} = t_0 + \Delta t_{fine}$ are obtained on fine grids.
4. Advect on fine grid ONLY.
5. Repeat steps 3 and 4. *N*-1 times.
6. Coalesce. The distributions pointing towards coarse grid are averaged on "overlapping" interface grids, resulting in the new incoming particle distributions for the coarse grid.
7. Go back to step 1.

where, "*N*" is the factor of refinement: $N = \delta x_{coarse} / \delta x_{fine}$.

Constraint is considered that the sound speed should be constant for both coarse and fine grids: $c_{sound} = \delta x_{coarse} / \delta t_{coarse} = \delta x_{fine} / \delta t_{fine}$. Therefore, the "operation" on fine grid is implemented N times for each coarse grid operation. For the sake of clarity, readers are suggested to refer to Chen et al. (2006) for details. In this study, *N* =4.

2.4 Wall boundary conditions

One of the advantages of LBM is its amazing simplicity for complex wall boundary condition treatments. The half-way bounce back wall condition might be the simplest and most widely accepted one, which could be used as an approximation of any wall profiles given grid refined enough. It is named "Boolean mask" in the Palabos - an open source code package. In this model, all the wall nodes are assumed to locate on half-way of the node-links. Some improvements of the model were proposed in recent years as well. However, the deficiency of the model is obvious and we still do not find any testing of the model for high Reynolds number flow. Based on the thought of bounce back, interpolated bounce back (IBB) method was proposed for curved boundary (Lallemand and Luo 2003b), which is regarded as one of the simplest models. The real wall position is considered in IBB, and the unknowns are interpolated according to the interior variables. The essence of IBB is to consider the standard lattice velocity (c_i) and it is applied to determine the original location of the particles which will be bounced back to the nodes neighboring to wall. For the reason of numerical stability, the interpolation is divided in two groups (as in Fig. 2):

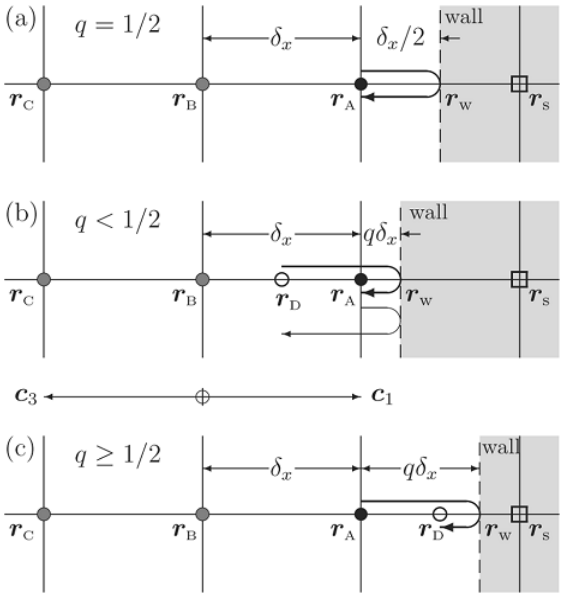

Fig. 2 Illustration of interpolated bounce-back boundary condition with q=1/2, q<1/2 and q>1/2.

$$f_{\bar{i}}(\boldsymbol{r}_A, t_n + \delta t) = q(2q+1) f_i^*(\boldsymbol{r}_A, t_n) + (1-4q^2) f_i^*(\boldsymbol{r}_A - \boldsymbol{c}_i \delta t, t_n) + q(2q-1) f_i^*(\boldsymbol{r}_A - 2\boldsymbol{c}_i \delta t, t_n) \quad \text{for } 0 < q < 0.5 \tag{6}$$

$$f_{\bar{i}}(\boldsymbol{r}_A, t_n + \delta t) = \frac{1}{q(2q+1)} f_i^*(\boldsymbol{r}_A, t_n) + \frac{(2q-1)}{q} f_{\bar{i}}^*(\boldsymbol{r}_A, t_n) + \frac{1-2q}{1+2q} f_{\bar{i}}^*(\boldsymbol{r}_A - \boldsymbol{c}_i \delta t, t_n) \quad \text{for } 0.5 < q < 1.0 \tag{7}$$

where f_i^* denotes the post-collision distribution function and quadratic interpolations are applied. And $q := \frac{|\boldsymbol{r}_A - \boldsymbol{r}_w|}{\delta x}$, $\boldsymbol{c}_i := -\boldsymbol{c}_{\bar{i}}$.

2.5 Far field boundary conditions

Non-reflective far field boundary conditions are suggested for open boundary problems with limited domain size. In present study, non-equilibrium extrapolated method (Guo et al., 2002) is applied at both inlet and outlet, which has been proven to have 1st and 2nd order accuracies for velocity and pressure boundary conditions (Shankar and Sundar 2009), respectively. It is constructed by the fact that density populations (f_i) are composed of equilibrium and non-equilibrium parts. The unknown incoming post collision populations are defined as,

$$\hat{f}_i^*(\rho, \boldsymbol{u}) = \hat{f}_i^{eq}(\rho, \boldsymbol{u}) + \left(1 - \frac{1}{\tau}\right) \hat{f}_i^{neq}(\rho, \boldsymbol{u}) \tag{8}$$

where the unknown macroscopic variables (ρ *or* $\boldsymbol{u}$) can be extrapolated from the interior nodes. The details could be found in Guo et al. (2002) and Shankar and Sundar (2009).

Compared to original model, additional treatments are needed to suppress the reflective pressure waves.

Absorbing layer was usually adopted for non-reflective boundary conditions. In Dirichlet conditions for velocities, like at inlet, density (pressure) can be extrapolated or calculated with the known interior distributions. In the scheme, the density is filtered in order to reduce the effect of pressure waves that reach the boundary. The proposed scheme involves filtering the density in time with a low-pass filter, so that the high frequencies are damped. Numerically, the procedure leads to a simple equation,

$$\bar{\rho}_{in} = \rho_{in}^n = \frac{\rho_e^n + T_c \rho_{in}^{n-1}}{1 + T_c} \tag{9}$$

where $\bar{\rho}_{in}$ is filtered density at the inlet at time step n, ρ_e^n the extrapolated value of density, such as thaton the fluid domain node next to the boundary, and T_c the empirical constant.

Following the idea of non-equilibrium extrapolated scheme, at outlet, the unknown velocity, u, is extrapolated from interior nodes next to the boundary. Although, the pressure is supposed to be fixed here, to reduce the reflected waves, a relaxation procedure, which is regarded as partial non-reflective condition (Finck et al., 2007), is adopted as follows

$$p_b^n = \frac{p_b^{n-1} + \rho c_s (u_n^n - u_n^{n-1}) + \alpha \Delta t p_{out}}{1 + \alpha \Delta t} \tag{10}$$

where p_{out} denotes the imposed pressure and u_n is extrapolated from inside to boundary. The new p_b^n is used in the non-equilibrium scheme.

3. RESULTS AND DISCUSSIONS

3.1 Validation of method and computation loads

With the aforementioned parameters, the flow around NACA0012 airfoil with Re=10^5 and AOA=4° is simulated. The corresponding vorticity and pressure contours and pressure coefficient, C_p, are shown in Fig. 3.

In the figure, dataset by Counsil and Boulama (2011) and that from FLUENT with SA turbulent model are compared. Six parameters sets (**P1~P6**) for LBM are adopted, the details of which are

Table 1 Computational parameters for IBB-LBM simulations.

	Cord length (c)	Wall distance(dw)	Airfoil location (d)	notes
P1	100	-	450	
P2	150	-	450	close to **P3**, not plotted
P3	200	-	450	
P4	200	- 25%	450	close to **P3**, not plotted
P5	200	-	400	
P6	200	-	300	

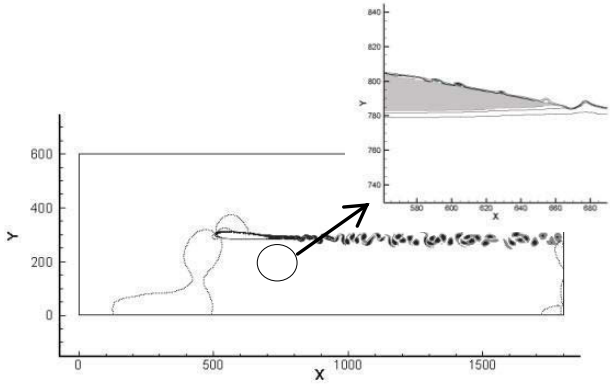

(a) Vorticity

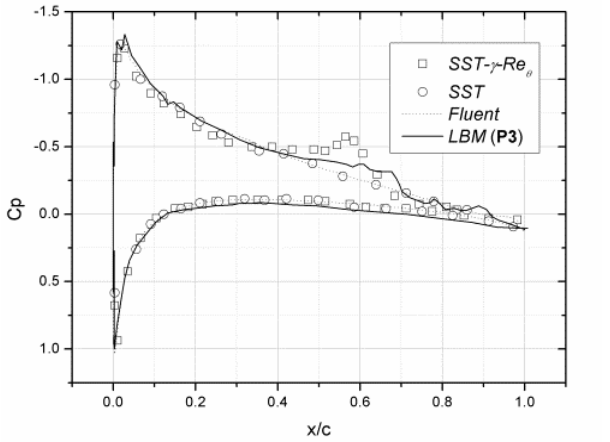

(b) Pressure

Fig. 3 Vorticity and pressure contours for flow around NACA0012 airfoil with Re=10^5 and AOA=4°. For pressure coefficients on surface of airfoil, □: SST-γ-Re_θ model (Counsil and Boulama, 2011), ○: SST model (Counsil and Boulama, 2011), ····· : SA model by FLUENT,—: LBM simulation (results of **P3** in Table 1).

listed in Table 1.The present results of **P2** and **P3** show quite good agreement with the previous ones. An interesting finding is that the flow separation is captured by LBM (streamlines are inserted in Fig. 3a), which is indicated in the pressure coefficient on the airfoil surface as well (Fig. 3b). It is similar to that from the more precise SST-γ-Re_θ model by Counsil and Boulama (2011), which is coincident with direct numerical simulation results. The analyses by Counsil and

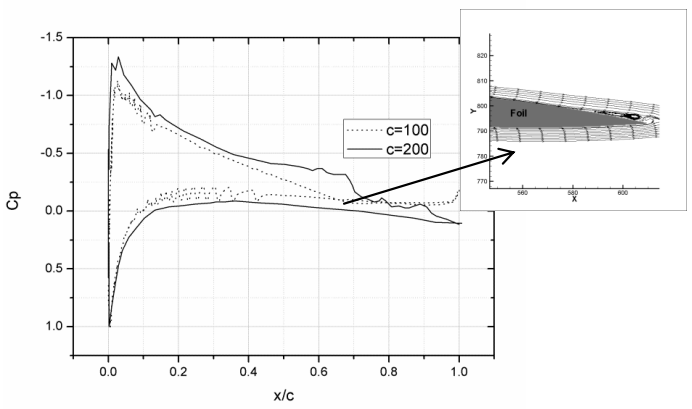

Fig. 4 Influences of grid resolution for LBM simulation: ····· :**P1**, —: **P3**(as in Table 1)**.**

Boulama (2011) and Rumsey and Spalart (2009) showed that both SST and SA turbulence models fail to predict flows for re-laminarization. Current model only has small differences in C_p value in the flow separation region. The reason of the discrepancy for SA model itself could be as follows.

1. In LBM, a square structure grid is applied, which has same resolution in both wall-normal and streamwise directions. In most traditional simulations, a stretched grid is applied in the region of boundary layer. Grid size influence is further tested with two coarser grids as "**P1**" and "**P2**" in Table 1, where the grid nodes on surface is $c \times N$ (N was defined in section 2.3).The location of flow separation is delayed only with parameter set "**P1**" (as in Fig 4 and Table 1).
2. The previous simulations were conducted in three dimensions, while currently two dimensional simulations are conducted.
3. As mentioned above, LBM is superior to traditional CFD method for turbulent flow. Some high order effects might play a role.

Further studies will be conducted in the future.
In this study the distance from first layer of grid nodes to wall (dw in Eq 3) is approximated simply by calculating the distance between "fluid" point to its closest "solid" node (see the pseudo-code in

section 3.2).The test of **P4** implies that the influence of incorrectness of "*dw*" can be neglected (Table 1). In **P4**, *dw* is reduced by 25%. Therefore, the slight incorrectness of "*dw*" can be accepted.

3.2 Performance of "Booleanmask" wall boundary treatments

Another comparison is carried out between "Boolean mask" and IBB wall boundary treatments. The former one roots in the simple half-way bounce back scheme, where the wall is assumed to locate on middle points of "solid"–"fluid" links. It is the simplest way to obtain a complex wall technically and is applied mostly in porous media flows. The question is how it works and whether we can apply it in high Reynolds number flows.

As we can imagine, an accurate simulation with "Boolean mask" wall depends on grid resolution strongly. Fig. 5 includes results with different grid resolutions. Although the trends of the pressure profiles are the same as the IBB one, apparent shifting of pressure and oscillations are observed.

Close looking shows flow separations are induced by the "stages". The biggest one is on the top of the foil, followed by a chain of small vortices (the left insert in Fig. 6), the core of which is always behind a stage. These vortices are stagnant, leading to pressure shifting. Downstream, several individual vortices are found as well (the middle insert in Fig. 6), which are caught by "stages". The numerous upstream vortices and staged wall profile suppress the vortex generation in IBB model and lead to a big stagnant vortex on the top surface of the tail (the right insert in Fig. 6). Therefore, certain discrepancies are observed for C_p.

In the testing range, increasing the grid resolution decreases the size and number of stagnant vortices. Comparatively more precise results are achieved consequently (simulations with foil resolved by 400 and 800 grids are presented in Fig. 5.). No large scale flow separations after $x/c \sim 0.5$ are found for "■" points in figure 5.For both tests, the error is difficult to be eliminated, especially on the top of the airfoil.

The pseudo-code to generate the foil "Boolean mask" is as follows.

```
// the wall locates on the halfway of links between wall and fluid nodes
if grid node is inside the foil, then
mask (node) = solid;
else
mask (node) = fluid;
end if.
…
dw = half of the distance from current "fluid" node to its closest "solid" node.
```

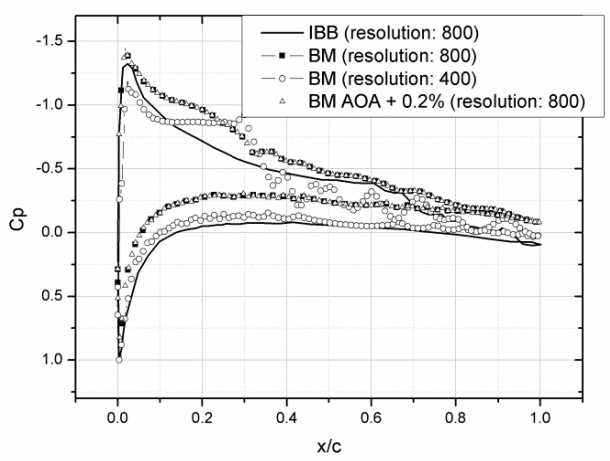

Fig. 5 Pressure coefficient with "Boolean mask" wall. Grid numbers on foil surface are 400 (○) and 800 (■) and with AOA (Δ) increased by 0.2% for comparison with IBB scheme.

If the conditional statements in codes are changed slightly, which will not influence the whole wall profile, the material state ("fluid" or "solid") on several individual nodes will change. The influences are explored by increasing AOA by 0.2%. However, that cannot make any apparent changes (Fig. 5), which implies the vortex is not induced by local effects, but by the patterns of "roughness" of the wall.

Consequently, although the feasibility of "Boolean mask" scheme for flows with high Reynolds number is questionable, it is believed that effects of wall roughness on flows can be explored with this method.

3.3 Analysis of feasibility of far field boundary conditions

As presented in section 2.5, density filter and relaxation approach are applied at inlet and outlet boundaries. The density distributions are shown in Fig. 7 during the establishment of the flow field. To illustrate the performance of the two approaches, the width of the computational domain (W) is shrunk. Partial reflectivity of the relaxation approach at outlet is demonstrated. As in Eq. 10, totally non-reflective condition could be obtained with α=0. However, this does not allow to properly impose the reference pressure. Fortunately, to capture the effects of periodically shed vortex, the computational domain is normally extended for downstream, and the wave will be damped further.

In the real calculation, since the flow in front of the foil is comparatively uniform and steady, the foil is usually much closer to the inlet. The noisy reflected waves are supposed to influence the convergence speed drastically. They are detected

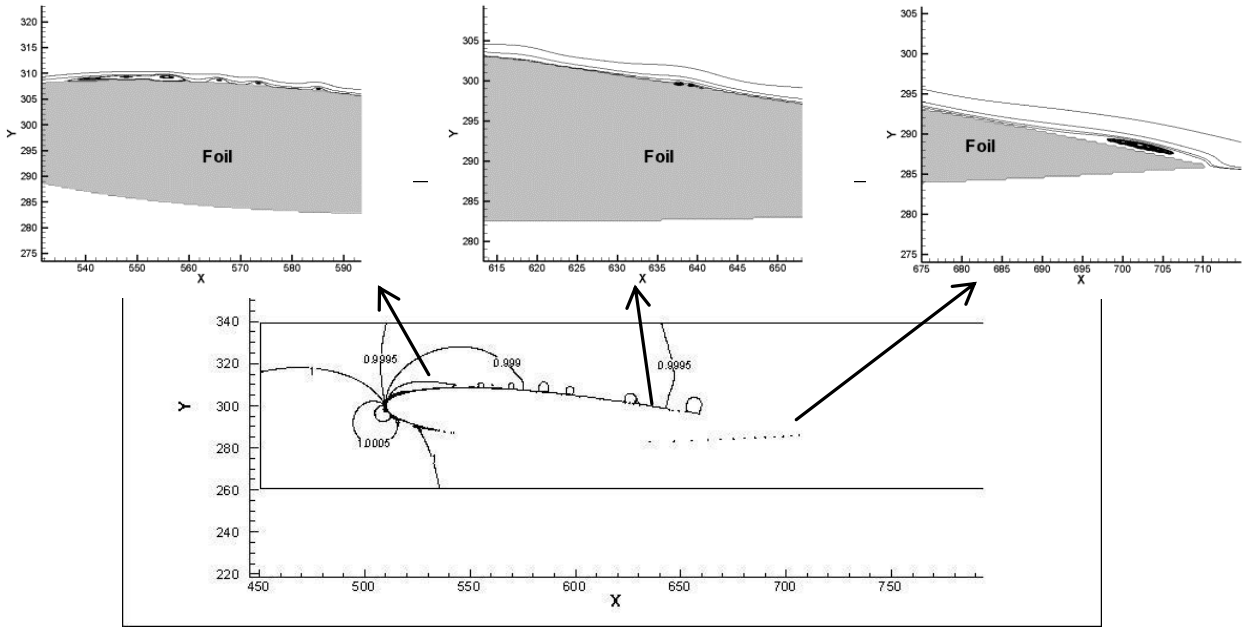

Fig.6 Density contours with "Boolean mask" wall and streamline around airfoil (surface of airfoil is resolved by 800 points).

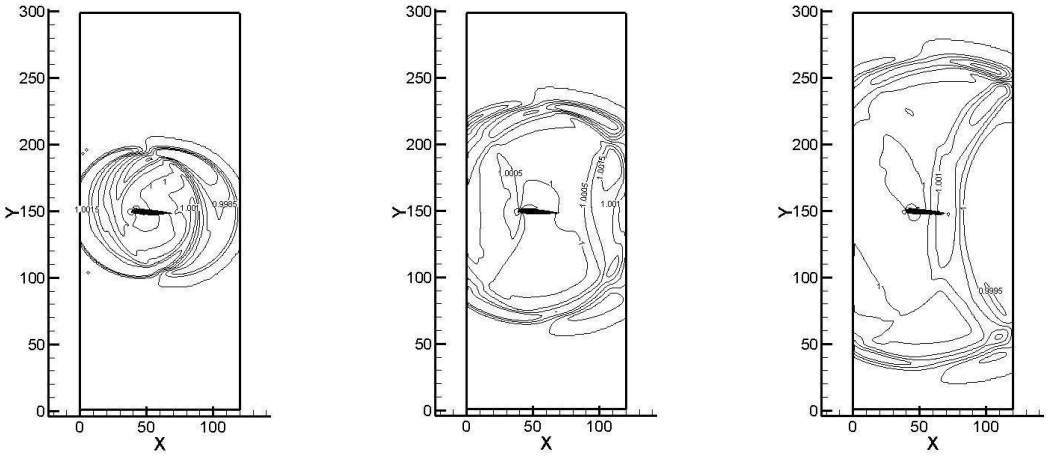

(a) (b) (c)

Fig. 7 Pressure wave propagation on stage of flow field establishment and wave damping boundary treatments, t=80, 140 and 200, from left to right.

clearly by Yu et al. (2003) and interpolation-based superposition scheme was proposed. However, it requires known inlet velocity and pressure, which is sort of inflexible for practical simulations. In the present study, incoming pressure wave almost disappears at inlet (Fig. 7c) with density filter approach, where Dirichlet velocity BC is imposed.

Further tests are implemented for the influences of the airfoil location. With the aforementioned inlet boundary performance, we believe that slightly changing the distance from inlet to airfoil tip (d) will not change the results, as **P5** and **P6** in Table 1. The pressure coefficient is illustrated in Fig. 8. When d~300, which corresponds to head inlet distance of 360, discrepancy is found. The main purpose of this test is to reduce the size of computational domain, and meanwhile, to demonstrate that the real flow conditions can be reproduced with well posed open boundary conditions. It should be noted that the distance from inlet to the head of foil is normally at least 8 times the cord length (Zhuo et al., 2010), and it is only 2~4 times in present study.

As a summary of this section, non-equilibrium extrapolated boundary scheme can be coupled with different kinds of boundary conditions. The wave damping approaches can reduce the reflected pressure waves and increase the convergence speed drastically.

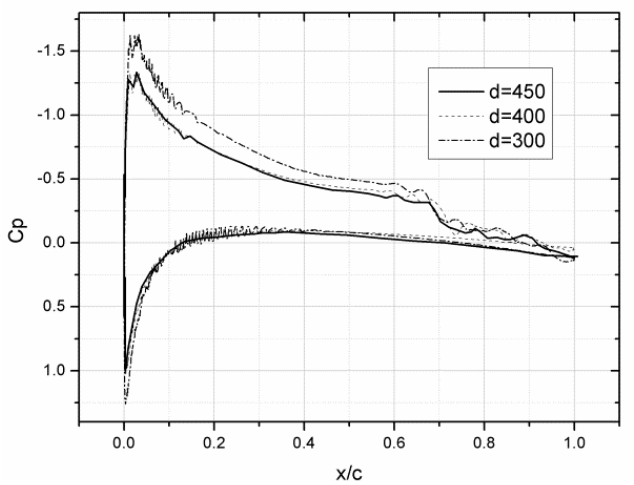

Fig. 8 Effects of location of foil, which is resolved by 800 grid points.

4. CONCLUSIONS

In this study, flows around NACA0012 are simulated with MRT-LBM methods coupled with SA turbulence model. Different computational aspects are discussed. The results are summarized as follows.

1. RANS turbulent model coupled with two dimensional LBM could predict flows with high Reynolds number precisely. With comparable grid resolution, traditional CFD methods fail to capture the flow separations with SA turbulence model. Meanwhile, the location of separation is caught correctly by present models, although the results show SA model produces in small discrepancy of C_p in the region of flow separation.
2. Well known "Boolean mask" boundary scheme is demonstrated to be unfeasible for high Reynolds number flow: vortices are induced by staged surface, which causes apparent errors for flow patterns and C_p. On the other hand, it is supposed to be able to explore the roughness effects of the wall.
3. Pressure wave damping schemes are incorporated with non-equilibrium extrapolation approach on open boundaries. The reflected waves are decreased drastically. The benefit is of two-folds, real flow condition can be reproduced, and computational resource can be saved.
4. Accordingly, MRT-LBM could be applied to high Reynolds number flows and after coupling with RANS turbulence model, 2D model can be readily implemented for certain preliminary studies.

ACKNOWLEDGEMENT

Support from NSF of China (Grant Nos. 10902087 and 11172241), Research Fund for Doctoral Programs of Higher Education of China, National Hi-Tech Development Programs of China (Grant No. 2012AA011803) and Key Laboratory of Hydrodynamics of China (partly) are gratefully acknowledged. The authors are grateful to Dr. Yan Peng at ODU for discussions. Parts of the computations was performed on Dawning-TC5000 system at Supercomputing Centre, Shenzhen Institute of Advanced Technology, CAS, China.

REFERENCES

1. Chen H, Filippova O, Hoch J et al (2006). Grid refinement in lattice Boltzmann methods based on volumetric formulation. *Physica A* 362:158-167.
2. Chen H, Kandasamy S, Orszag S, et al (2003). Extended Boltzmann kinetic equation for turbulent flows. *Science* 301:633-636.
3. Chen SY, Doolen GD (1998). Lattice Boltzmann method for fluid flows. *Annu. Rev. Fluid Mech* 30:329-364.
4. Chen XP, Zhong CW, Yuan XL (2011). Lattice Boltzmann simulation of cavitating bubble growth with largedensity ratio. *Comput. Math. Appl.* 61:3577-3584.
5. Counsil JNN, Boulama KG (2012). Validating the URANS shear stress transport γ-Re_θ model for low-Reynolds-number external aerodynamics. *Int. J. Num. Method Fluids* 69:1411-1432.
6. Estallo SI (2008). *Computational Gas Dynamics with the Lattice Boltzmann Method*. PhD. Dissertation, Universidad de Zaragoza.
7. Filippova O, Succi S, Mazzocco F, Arrighetti C, Bella G, Hänel D (2001). Multiscale lattice Boltzmann schemes with turbulence modeling. *J. Comput. Phys.* 170:812-829.
8. Finck M, Hanel D, Wlokas (2007). Simulation of nasal flow by lattice Boltzmann methods. *Comput. Bio. Med.* 37:739-749.
9. Guo Z, Zheng C, Shi B (2002). An extrapolation method for boundary conditions in lattice Boltzmann method. *Phys Fluid* 14(6):2007-2010.
10. d'Humieres D (2002). Multiple- relaxation-time lattice Boltzmann models in three dimensions. *Phil. Trans. Roy. Soc. A* 360:437-451.

11. Kam EWS, So RMC, Leung RCK (2007). Lattice Boltzmann Method simulation of aeroacoustics and nonreflecting boundary conditions. *AIAA J.* 45(7):1703-1712.
12. Lallemand P, Luo L-S (2003a). Theory of the lattice Boltzmann method: Acoustic and thermal properties in two and three dimensions. *Phys. Rev. E* 68:036706.
13. Lallemand P, Luo L-S (2003b). Lattice Boltzmann method for moving boundaries. *J. Comput. Phys.* 184:406-421.
14. Liu M, Chen XP, Premnath KN (2012). Comparative study of the large eddy simulations with the lattice Boltzmann method using the wall-adapting local eddy viscosity and Vreman subgrid scale models. *Chin. Phys. Lett.* 29(10):104706.
15. Premnath KN, Pattison MJ, Banerjee S (2009). Generalized lattice Boltzmann equation with forcing term for computation of wall-bounded turbulent flows. *Phys. Rev. E* 79:026703.
16. Rumsey CL, Spalart PR (2009). Turbulence model behavior in low Reynolds number regions of aerodynamic flow fields. *AIAA J.* 47(4):982-993.
17. Scagliarini A, Biferale L, Sbragaglia M, Sugiyama K, Toschi F (2010). Lattice Boltzmann methods for thermal flows: Continuum limit and applications to compressible Rayleigh–Taylor systems. *Phys Fluid* 22:055101.
18. Shankar M, Sundar S (2009). Asymptotic analysis of extrapolation boundary conditions for LBM. *Comput. Math. Appl.* 57:1313-1323.
19. Spalart PR (2000). Strategies for turbulence modeling and simulations. *Int. J. Heat Fluid Flow* 21:252-263.
20. Yu D, Mei R, Luo L-S, Shyy W (2003). Viscous fl20 computations with the method of lattice Boltzmann equation. *Proc. Aerospace Sci.* 39:329-367.
21. Zhuo C, Zhong CW, Li K, Xie J, Zhang Y (2010). Simulation of high Reynolds number flow around airfoil by lattice Boltzmann method. *Acta Aeronaut. Astronaut. Sinica* 31(2):238-243. (in Chinese)